JOURNAL OF THERMOPHYSICS AND HEAT TRANSFER
Vol. 20, No. 3, July–September 2006

# Film-Cooling Prediction on Turbine Blade Tip with Various Film Hole Configurations

Huitao Yang,* Hamn-Ching Chen,† and Je-Chin Han‡
*Texas A&M University, College Station, Texas 77843-3123*

**Different film hole arrangements on the plane and squealer tips of a turbine blade are investigated using a Reynolds stress turbulence model and nonequilibrium wall function. The three film hole configurations considered are 1) the camber arrangement, where the film-cooling holes are located on the mid-camber line of the tips; 2) the upstream arrangement, where the film holes are located upstream of the tip leakage flow and high heat transfer region; and 3) the two-rows arrangement, which is a combination of the camber and upstream arrangements. Calculations were performed first for the nonrotating cases under low inlet/outlet pressure ratio conditions with three different blowing ratios. The predicted heat transfer coefficients are in good agreement with the experimental data, but the film-cooling effectiveness is somewhat overpredicted downstream of the film holes. Simulations were then performed for the nonrotating and rotating camber line film hole configuration under high inlet/outlet pressure ratio conditions, which are close to engine conditions. It is found that the rotation decreases the plane tip film-cooling effectiveness but only slightly affects the squealer tip film cooling. However, the rotation significantly increases heat transfer coefficient on the shrouds.**

## Nomenclature

$h$ = local heat transfer coefficient, $q_w/(T_w - T_{t\infty})$, W/m$^2\cdot$K
$M$ = global film coolant blowing ratio, $(\rho_c V_c)/(\rho_{av} V_{av})$
$P$ = local static pressure, Pa
$P_t$ = inlet total pressure, Pa
$St$ = Stanton number, $h/(\rho_{in} v_{in,relative} C_p)$
$Tu$ = inlet turbulence intensity level, %
$X$ = axial distance, cm
$\eta$ = adiabatic film cooling effectiveness, $(T_{t\infty} - T_{aw})/(T_{t\infty} - T_c)$
$\theta$ = dimensionless temperature field, $(T - T_c)/(T_{t\infty} - T_c)$
$\rho$ = density, kg/m$^3$

*Subscripts*

av = average of cascade inlet and outlet
aw = adiabatic wall
$c$ = coolant
$t$ = total or stagnation value
$w$ = wall of blade and shroud
$\infty$ = inlet stream of cascade

## I. Introduction

TURBINE blade tips are exposed to high heat load due to strong tip leakage flow, which greatly affects the overall life and performance of a gas turbine. A common way to provide adequate cooling of the blade tips is to extract some cooling air from the coolant passages, through the film holes, to protect tip surface from the hot leakage gas. The goal of turbine designer is to optimize the film cooling for a limited amount of coolant because the same coolant air from the compressor can be used to generate the power or thrust. To achieve this goal, it is important to study systematically the arrangement of film holes, the associated blowing ratio, and the tip structure affecting the film-cooling effectiveness and heat transfer coefficient. At present, most experiments of film cooling on the turbine blades can only be performed for the nonrotating cases with a relative low cascade inlet/outlet pressure ratio due to the limitation of test rigs. To use these experimental data for film-cooling applications under real engine conditions, it is desirable to employ advanced numerical methods that are capable of simulating the effects of blade rotation and high cascade inlet/outlet pressure ratio for practical engine operation conditions.

There have been numerous studies that addressed the heat transfer and film cooling on the blade tip. Metzger et al.[1] and Chyu et al.[2] investigated heat transfer in a rectangular grooved tip model. Their studies include the effect of the depth and gap to the width ratio of a cavity with both moving and standing shrouds over the stationary grooved tip model. Kim et al.[3] presented a summary of the heat transfer coefficient and film cooling on a blade tip model studied by Metzger. Bunker et al.[4] studied the detailed heat transfer distribution on a blade tip of a power-generation gas turbine. Bunker and Bailey[5] studied the effect of squealer cavity depth and oxidation on turbine blade tip heat transfer. Dunn and Haldeman[6] measured time-averaged heat flux at recessed blade tip for a full-scale rotating turbine stage at transonic vane exit conditions. Bunker[7] provided a comprehensive review and summary of the blade tip heat transfer.

Experimental studies have also been carried out by Azad et al.[8,9] using a transient liquid crystal technique (LCT) to study the heat transfer and pressure distributions on a GE-E$^3$ blade with plane and squealer tips. Saxena et al.[10] investigated the effect of various tip sealing geometries on the blade tip leakage flow and heat transfer of a scaled up high pressure turbine blade in a low-speed wind tunnel facility using a steady state hue, saturation, and intensity-based LCT. They found that the trip strips placed against the leakage flow produce the lowest heat transfer on the tips compared to the other cases. Kwak et al.[11] studied the effect of squealer geometry arrangements on the blade tip leakage flow and heat transfer in a high-speed blowdown cascade facility using the hue detection-based transient LCT. They found that the suction-side squealer tip provided the lowest heat transfer coefficient on the blade tip and near tip regions compared to the other squealer geometry arrangements.

Numerical studies to investigate blade tip heat transfer have also been conducted. Ameri et al.[12] predicted the effects of tip gap clearance and casing recess on heat transfer and stage efficiency for several squealer blade tip geometries. Ameri and Rigby[13]

Received 25 June 2005; revision received 21 November 2005; accepted for publication 5 December 2005. 

*Research Assistant, Turbine Heat Transfer Laboratory, Department of Mechanical Engineering; yang@tamu.edu. Student Member AIAA.
†Professor, Ocean Engineering Program, Department of Civil Engineering; hcchen@civil.tamu.edu. Senior Member AIAA.
‡M.C. Easterling Chair Professor, Turbine Heat Transfer Laboratory, Department of Mechanical Engineering; jc-han@tamu.edu. Associate Fellow AIAA.

also calculated heat transfer and film-cooling effectiveness on film-cooled turbine blade models. Ameri and Bunker[14] investigated the detail heat transfer distributions on blade tip surfaces for a large power-generation turbine blade and compared the results with the experimental data of Bunker et al.[4] Ameri[15] predicted heat transfer and flow on the blade tip of a gas turbine equipped with a mean-camber line strip.

The experimental results of Azad et al.[8,9] have been investigated numerically by Yang et al.,[16,17] and a good agreement was found in the heat transfer distribution. Both the experiment and the numerical calculations have found that a high heat transfer coefficient is located on the pressure side of the plane tip and on the leading and suction portion of the cavity bottom of squealer tip. The squealer tip can reduce the heat transfer and leakage flow velocity.

Kwak and Han[18,19] used the transient liquid crystal method to investigate the film cooling with 13 film holes located along the camber line of the GE-E$^3$ blade tip. They concluded that the coolant injection slightly reduces the heat transfer coefficient downstream of the film holes, the film-cooling effectiveness increases with increasing blowing ratio for all cases, and the squealer tips have higher cooling effectiveness compared with plane tips. Most important, their study also indicated that the camber line film-hole arrangement does not provide adequate protection for the high heat transfer areas on either the plane or squealer blade tips because the film cooling is effective only on the downstream side of the tip leakage flow, where the heat transfer coefficients are relatively low. Acharya et al.[20] performed numerical simulation of film cooling on GE-E$^3$ plane and squealer tips for the same GE-E$^3$ blade of Kwak and Han[18,19] but with only seven film holes along the camber line of the blade tip. Their numerical studies indicated that the film coolant acts as a blockage to the tip leakage flow due to the lower coolant velocity compared to the tip leakage flow, the coolant trajectory is directed from the pressure side to the suction side for the plane tip, but it rolls inside the cavity from suction side to the trailing edge for the squealer tip, the film-cooling effectiveness of tip and shroud increases with increasing blowing ratio, and the film cooling generally decreases the heat transfer downstream of the film holes instead of increasing it as observed in other film-cooling applications. Recently, Hohlfeld et al.[21] predicted film-cooling flow from dirt purge holes on the tip of a turbine blade using the FLUENT computational fluid dynamics code (CFD) code. They found that the flow exiting the dirt purge holes act as a blockage for the leakage flow across the gap. As the blowing ratio increased for a large tip gap, the tip cooling increases only slightly while the cooling to the shroud increases significantly.

The present study focuses on the optimization of film-hole arrangements on both the plane and squealer tips of the GE-E$^3$ blade using the Fluent CFD code with Reynolds stress turbulence model and nonequilibrium wall function. Detailed validations of the present numerical method and turbulence model for blade tip leakage flow were presented by Yang et al.[16,17,22] In general, the predicted heat transfer coefficients are in good agreement with the experimental data of Azad et al.[8,9] and Kwak and Han.[18,19] For the film-cooling effectiveness on the blade tip, however, no direct comparisons of the simulation results with the experiment have been reported in the open literature so far. In this paper, numerical simulations are performed and compared with the experimental data obtained using pressure sensitive paint (PSP) technique by Ahn et al.[23] The previous studies by Yang et al.[16,17] showed that the Reynolds stress turbulence model provides somewhat more accurate resolution of the complex flow inside the squealer cavity. Therefore, this Reynolds stress model is used together with the nonequilibrium wall function for the near-wall region. There were only a few studies addressing film cooling and the associated heat transfer coefficient on blade tips, and the effects of film-hole locations and blade rotation have not been systematically studied. Therefore, the work presented here is unique to the literature.

## II. Arrangements of Film Holes on Blade Tip

The original design of the holes on the blade tip is used to purge dirt from the coolant by centrifugal force, such that these dirt particles will not block the small diameter film holes. Most often, these holes are arranged on the midcamber line of the tips due to manufacturing reasons. However, this simple camber line film-hole arrangement may not yield a good design for blade tip film-cooling applications because the film-cooling jets do not provide adequate coverage for the high heat transfer regions on either the plane or squealer blade tips. For example, Fig. 1 shows the measured film-cooling effectiveness and heat transfer coefficients for the camber line film-hole arrangements on plane and squealer tips as tested by Kwak and Han.[18,19] For the plane tip case, the high heat transfer region was observed on the pressure side of the blade tip. However, the film coolant jets were bent toward the suction portion of the blade tip and did not provide good protection on the pressure-side high heat transfer region. For the squealer tip case, the high heat transfer region is located near the leading edge and along the suction side of the squealer cavity floor. However, the coolant jet was pushed toward the pressure side of the cavity with poor protection on the suction-side high heat transfer region. In both the plane and squealer tips, the film coolant covers only one-half of the blade tip downstream path of the film-coolant jets. The portion upstream path of the film holes does not benefit from the film cooling.

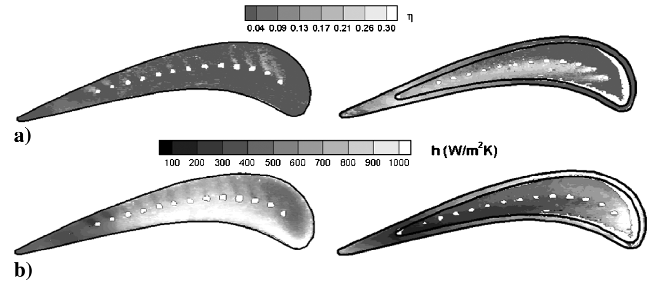


**Fig. 1 Film-cooling effectiveness and heat transfer coefficient distribution of camber arrangement on plane tip (left) and squealer tip (right). a) film cooling effectiveness, $M = 1$ and b) heat transfer coefficient, $M = 1$. (Kwak and Han[18,19]).**

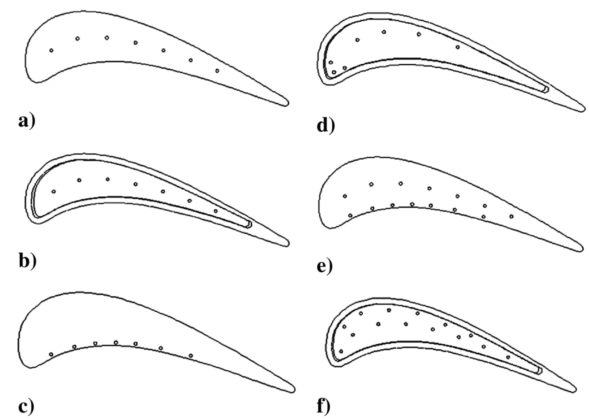


**Fig. 2 Various film hole arrangements: a) camber plane tip, b) camber squealer tip, c) upstream plane tip, d) upstream squealer tip, e) two-row plane tip, and f) two-row squealer tip.**

To compare film-cooling performance on the blade tip, three different film-hole arrangements were investigated in the present study, as shown in Fig. 2. Figures 2a and 2b, for the plane and squealer tips, denoted the camber arrangement, serve as a baseline for comparison. The film-hole geometry and camber arrangements are identical to the experimental geometry reported by Ahn et al.[23] The locations of the film holes shown in Figs. 2c and 2d were selected based on the implication of the film-cooling and heat transfer results presented in Fig. 1 by Kwak and Han,[18,19] the local blade tip heat transfer coefficients presented by Azad et al.,[8,9] and the blade tip leakage flow patterns obtained from previous numerical studies by Yang et al.[16,17] For example, Fig. 3 shows the predicted pathlines of tip leakage flow for both the plane and squealer blade tips. For the plane tip in Fig. 3a, the tip leakage flow is driven by the pressure gradients from the pressure side to the suction side and the high heat transfer

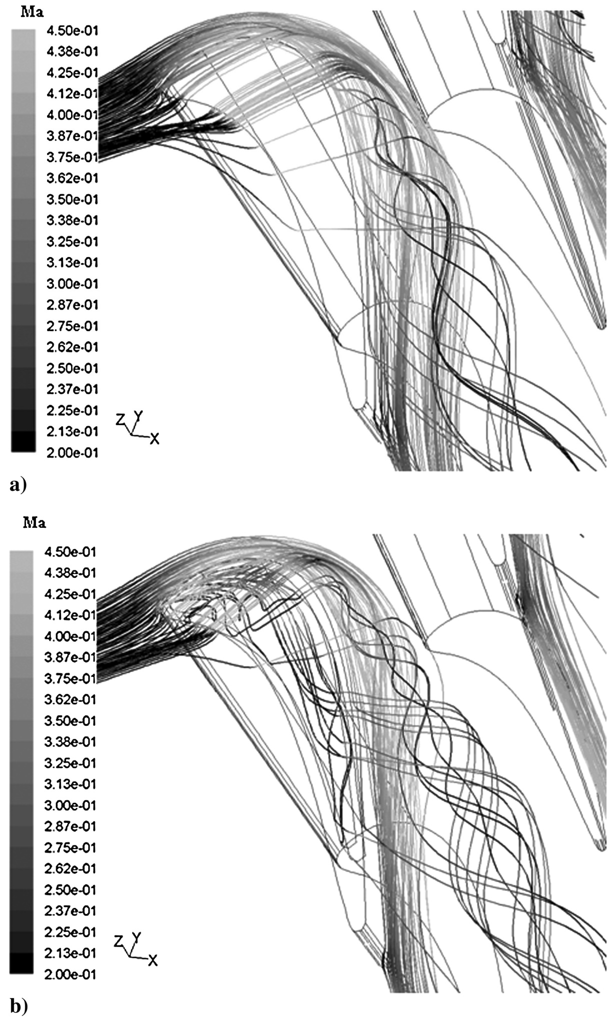


**Fig. 3 Comparison of tip leakage flow pathlines (shaded by Mach number) between a) plane tip (Yang et al.[16]) and b) squealer tip (Yang et al.[17]) configurations.**

region is located near the pressure side on the blade tip. The predicted tip leakage flow pathlines explained fairly well the local heat transfer data presented by Azad et al.[8] and Kwak and Han.[18] An effective way to improve the film-cooling effectiveness is to locate the film holes on the plane tip near the pressure side to provide more coverage of the blade tip region, as shown in Fig. 2c. For the squealer tip, the leakage flow is much more complex compared to the plane tip case, especially inside the squealer cavity. The computed pathlines in Fig. 3b show that the squealer tip leakage flow moves over the squealer rim on the pressure side, rolls down inside the cavity, then rolls up again to leave the cavity over the suction side of the squealer rim near the trailing edge. Consequently, a high heat transfer region was observed along the suction side of the squealer cavity. In addition, another high heat transfer region was dictated near the leading edge inside the squealer cavity due to the reattachment of the blade tip leakage flow. This leakage flow pattern also provides a good explanation of the local heat transfer data presented by Azad et al.[9] and Kwak and Han[19] for the squealer tip configuration. Based on the preceding observations for squealer tip leakage flow and heat transfer coefficient distributions, it is proposed to place three film holes near the leading edge of the blade tip inside the cavity to provide better protection for the high heat transfer region around the blade leading edge. The other four holes are located near the suction side to provide better film-cooling coverage for the other high heat transfer region along the suction side of the blade tip, as shown in Fig. 2d. The preceding two film-hole arrangements for the plane and squealer tips are denoted as upstream arrangements, as shown in Figs. 2c and 2d because the film holes were placed strategically on the upstream of the tip leakage flow and the high heat transfer areas.

In addition, it is desirable to investigate whether one row or two rows of film holes will provide better film cooling for the same amount of given coolant flow rate. In the present study, two different kinds of two-row film hole arrangements were investigated for the plane and squealer tips, respectively. For the plane tip case, one row of seven film holes was located on the camber line, whereas another row of seven holes was placed near the pressure side, as shown in Fig. 2e. This is essentially a combination of the camber line and upstream arrangements to provide better film-cooling coverage for the entire blade tip. A different two-row arrangement was proposed for the squealer tip case, as shown in Fig. 2f. In this arrangement, one row with seven film holes was located along the suction side of the squealer cavity upstream of the leakage flow inside the cavity, whereas the other row of seven holes was placed along the camber line. To provide a fair comparison of the film-cooling effectiveness, the total amount of coolant is maintained the same for all film-hole arrangements considered in the present study. This implies that the averaged local blowing ratio for the two-row configurations is only one-half of those considered in the camber and upstream film-hole configurations.

## III. Computational Details

The simulations were performed using the CFD software package Fluent[24] (version 6). The solutions were obtained by solving the compressible Reynolds-averaged Navier–Stokes equations using a finite volume method to discretize the continuity, momentum, and energy equations. GAMBIT software was used to generate the unstructured hexahedron grids, with fine grid clustering inside the blade boundary layer and the blade tip region. Figure 4a shows a typical film-cooled squealer tip blade with selected cross-sectional planes, which will be used later to show the secondary flow structures around the blade tip region. Unlike the earlier study of Acharya et al.,[20] which used long cylindrical tubes to represent the film holes, a coolant plenum and two coolant passages are included in the present simulations to provide a more realistic representation of the blade tip film-cooling configuration.

Relatively coarse grids are used inside the coolant passages and the plenum, whereas the film holes and squealer tip regions are covered with much finer grids for accurate resolution of the film-cooling jets and tip leakage flows. The value of $\boldsymbol{y}^*(=\boldsymbol{C}_\mu^{1/4}\boldsymbol{k}_p^{1/2}\boldsymbol{y}_p/\boldsymbol{\nu})$ for the nonequilibrium wall function falls between 25 and 100 for most of the blade tip region, where $\boldsymbol{k}$ is the turbulent kinetic energy and the subscript $p$ denotes the near-wall grid point. The geometry and detailed numerical grids around a typical film-cooled squealer tip is shown in Fig. 4b. Similar grid structures were used for the other film-hole arrangements.

The present calculations were carried out for a three times scaled-up model of the GE-E$^3$ blade. This blade configuration is identical to that used in the experimental study of Kwak and Han.[18,19] The scaled-up blade has an axial chord length of 8.61 cm, and the aspect ratio of the span to the chord is 1.4. The blade leading-edge pitch is 9.15 cm. The tip clearance studied here is 1.97 mm, that is, 1.5% of the blade span. For the squealer tip, the depth of the cavity is 4.6 mm, which is 3.77% of the blade span, and the cavity rim width is 2.54 mm. The diameter of the film holes is 0.127 cm.

The computational domain consists of a single blade with periodic boundary conditions imposed in the circumferential direction. At the inlet, the total temperature, 300 K, total pressure, 129.96 kPa, and static pressure, 124.43 kPa, are specified with an inlet flow angle of 32 deg. The inlet turbulence intensity is taken as 9.7%. At the exit, the static pressure is specified as 108.3 kPa. All of these flow conditions are identical to the experimental setup of Kawk and Han[18,19] and Ahn et al.[23] Three global blowing ratios of $M = 0.5$, 1.0, and 2 have been studied with fixed mass flux boundary conditions. To calculate the film-cooling effectiveness, the coolant temperature is taken as 350 K and the turbulence intensity is $Tu = 3\%$, the same as those given by Kwak and Han,[18,19] and the adiabatic boundary condition is used on the blade and shroud surfaces. To calculate the heat transfer, a different thermal boundary condition is used with the wall temperature fixed at 350 K and the inlet coolant temperature is maintained the same as the cascade inlet temperature.

For completeness, simulations were also performed for the same three times scaled-up GE-E$^3$ blade using typical operating conditions for a real turbine with a blade tip radius of 35.56 cm (14 in.) under both nonrotating and rotating conditions. This enables us to evaluate the effects of rotation, high temperature, high Mach number, and high cascade inlet/outlet pressure ratio on the film-cooling effectiveness and heat transfer in the blade tip region. A rotating speed of 9600 rpm (1005.31 rad/sec.) is used in the present rotating blade simulation. The inlet total temperature is specified at 1700 K, and the coolant temperature is 923 K for the film-cooling effectiveness calculation. To calculate the heat transfer coefficient, the coolant temperature is kept the same as the cascade inlet temperature of 1700 K, whereas the blade surface temperature is specified at 1190 K. The inlet turbulence intensity is 9.7%, and the inlet flow angle is 32 deg. The total pressure at the inlet is 1.675 MPa, and the static pressure at the exit is 1.03 MPa. This gives an inlet/outlet pressure ratio $P_{\mathrm{in},t}/P_{\mathrm{out}}$ of 1.63, which is significantly higher than the 1.2 used in the experiments of Kwak et al.[13,14] For convenience, the simulations at high total temperature and high inlet/outlet pressure ratio cases are denoted as high parameter, whereas the low inlet/outlet pressure ratio and low total temperature cases corresponding to the experimental conditions are denoted as low parameter in the following discussions. For the rotating cases, the whole blade domain is rotating with a relative inlet flow angle equal to 32 deg, whereas the shroud remains stationary. All other conditions are kept the same as the high parameter stationary case to facilitate a detailed understanding of the effects of blade rotation under realistic turbine working conditions.

All calculations are converged to residual levels of the order of $10^{-5}$ and to less than 0.1% error in the mass flow rate between the cascade mainstream flow and film coolant inlet and outlet of the computational domain. Typically, 800 iterations are needed to achieve the desirable convergence. Grid-refinement studies have been performed for all cases using at least two different grid densities. Figure 5 shows the cooling effectiveness on the squealer tip for three different grids with 0.74, 1.1, and 1.5 million grid points, respectively. The change of the film-cooling effectiveness between the intermediate and fine grid solutions is fairly small, indicating that the finest grid solution is nearly grid independent. As shown in Table 1, a total of 20 simulations were performed for the nonrotating low parameter cases with various combinations of blade tip geometry, film-hole arrangement, and blowing ratio. In addition, eight high

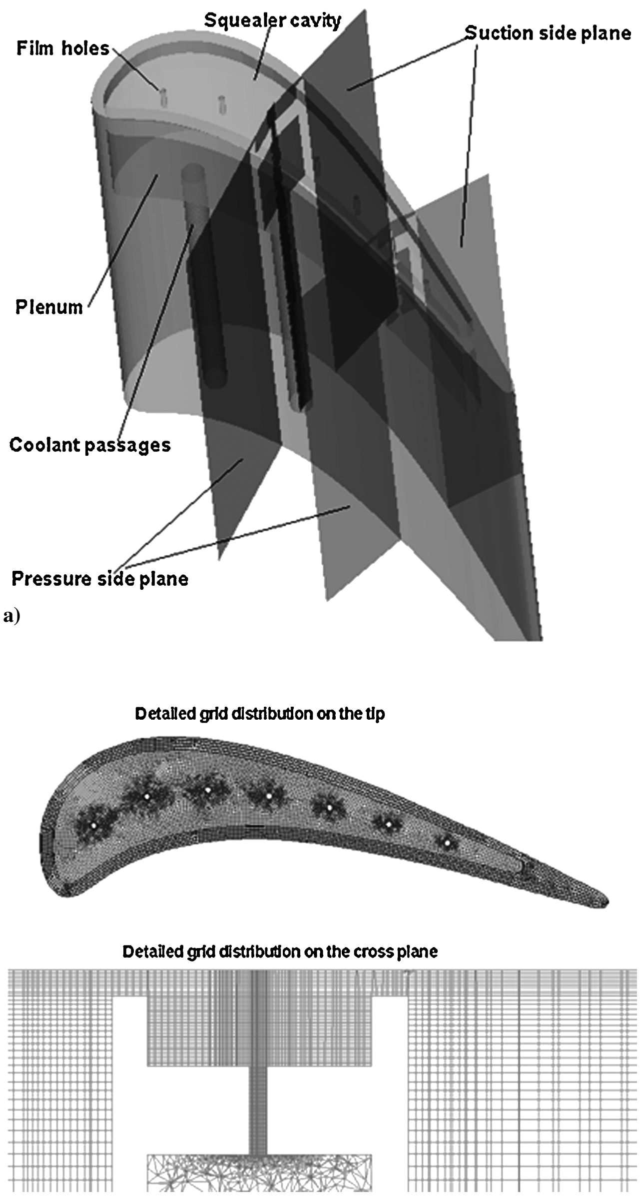


Fig. 4 Geometry and numerical grids: a) schematic of typical film cooled GE-E$^3$ blade with squealer tip and selected cross sections and b) detailed grid distribution of the film-cooled squealer tip and film hole.

**Table 1 Matrix of numerical simulations**

| | Plane tip | | | Squealer tip | | |
|---|---|---|---|---|---|---|
| Approximate grid number (million) | Camber 0.9 | Upstream 1 | Two rows 1.3 | Camber 1.5 | Upstream 1.6 | Two rows 1.7 |
| *Film-cooling effectiveness* | | | | | | |
| Low parameter, nonrotating | | | | | | |
| $M = 0.5$ | × | × | × | × | × | × |
| $M = 1$ | × | × | × | × | × | × |
| $M = 2$ | × | × | × | × | × | × |
| High parameter, nonrotating | | | | | | |
| $M = 1$ | × | | | × | | |
| High parameter, rotating | | | | | | |
| $M = 1$ | × | | | × | | |
| *Heat transfer coefficient* | | | | | | |
| Low parameter, nonrotating | | | | | | |
| $M = 1$ | × | | | × | | |
| High parameter, nonrotating | | | | | | |
| $M = 1$ | × | | | × | | |
| High parameter, rotating | | | | | | |
| $M = 1$ | × | | | × | | |

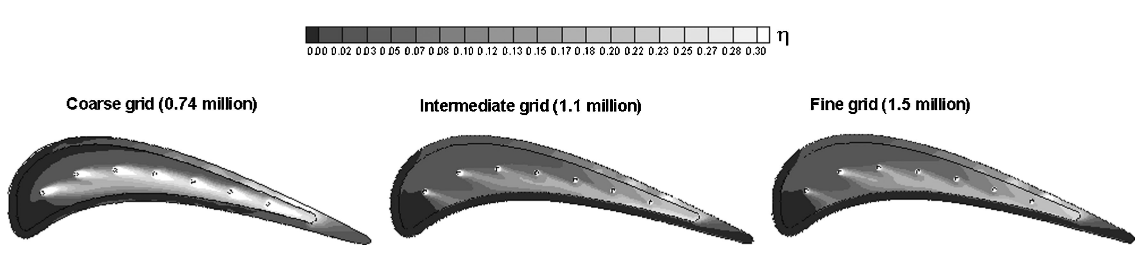


Fig. 5 Grid-refinement study.

parameter cases were also investigated for the plane and squealer tip configurations blade tip cooling configurations under nonrotating as well as rotating conditions. A systematic grid refinement study was performed for all cases, but only the finest grid results are presented in this paper.

## IV. Results and Discussion

### A. Distribution of Pressure Ratio

Figure 6 shows a comparison of the predicted pressure ratio $P_t/P$ distribution for camber line, upstream, and two-row film-hole arrangements. Generally speaking, the high-pressure ratio means low local static pressure and high velocity. For the plane tip configurations, it is clearly seen that the pressure ratio is relatively low, that is, low velocity, upstream of the coolant jet, whereas high-pressure ratios were observed downstream of the coolant jet. This indicates that the coolant velocity is slower than the surrounding fluid and acts as an obstacle to the surrounding tip leakage flow. The effect of jet blockage on the tip leakage flow is considerably weaker for the squealer tip due to the large squealer cavity depth. The simulation results show that the pressure ratio on the plane tip is strongly affected by different film-hole arrangements. In particular, the upstream arrangement produced a significantly higher pressure ratio than the other two film-hole arrangements. On the other hand, the effect of film cooling on the squealer tip is considerably weaker than that of the plane tip because the cavity depth is much larger than the plane tip clearance. Also note that the computed leakage flow velocity in the tip clearance is significantly higher than the cascade average velocity for both the plane and squealer tip configurations because the leakage flow is driven by strong pressure gradients across the tip clearance.

Figure 7 shows a comparison of the computed pressure ratio contours with the PSP data of Ahn et al.[23] on the shrouds for the blowing ratio $M = 1$ cases. In general, the predicted trends of pressure ratio match well with the corresponding measurement. The highest pressure ratio value measured by the PSP is about 1.25 in the plane tip region, whereas the predicted maximum pressure ratio is slightly higher at 1.3. For the squealer tips, the highest pressure ratio above the cavity is about 1.19, whereas the predicted value is about 1.2 at the same location. Experimental PSP data show that the effect of film cooling is negligible on the shroud, whereas the simulations indicated the presence of strong film-cooling effects on the shroud for the plane tip cases. Both the experiments and simulations show that the squealer tips reduce the tip leakage flow velocity significantly due to flow separation and recirculation in the squealer cavity. Because the plane tip clearance is much smaller than the depth of the squealer cavity, the effect of plane tip film cooling on the shroud is stronger than that observed for the squealer tip cases. In addition, the tip leakage vortex is affected by different film-hole arrangements, especially for the plane tip due to the small

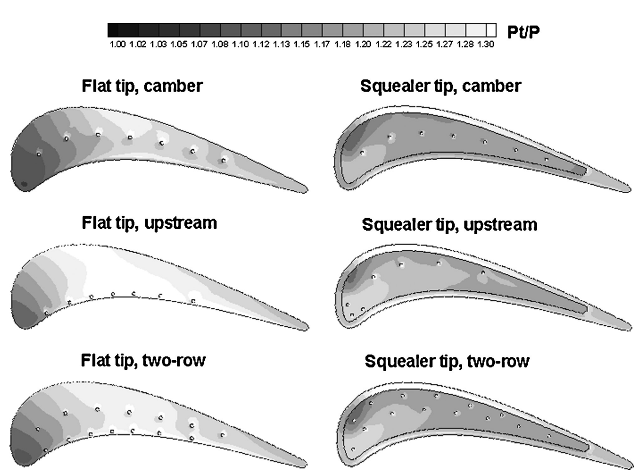


**Fig. 6 Comparison of pressure ratio $P_t/P$ distributions on plane and squealer tips among various low parameter film-hole arrangements; $M = 1$ for camber and upstream configurations and $M = 0.5$ for two-row configuration.**

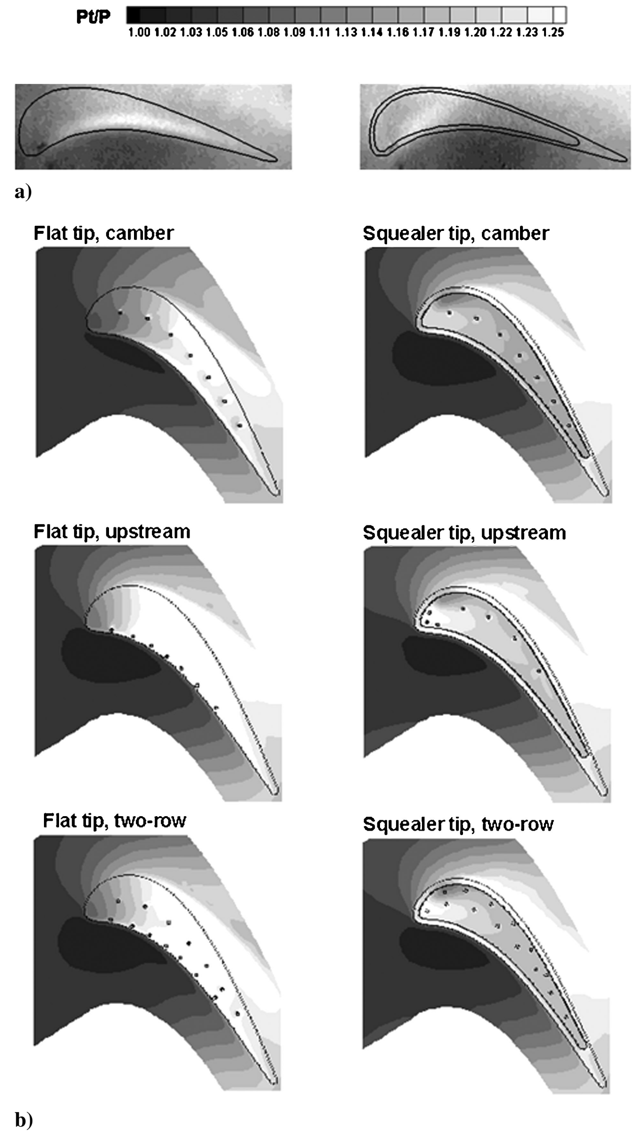


**Fig. 7 Pressure ratio $P_t/P$ distributions on shrouds among various low parameter plane tip (left) and squealer tip (right) configurations and film hole arrangements $M = 1$ for camber and upstream configurations and $M = 0.5$ for two-row configuration: a) Ahn et al.[23] experimental PSP data and b) numerical simulation.**

tip gap. Note that the trajectory of the tip leakage vortex can be traced by the shape of the pressure ratio contours near the blade suction side of the shroud surface, which is dictated by both experiment and numerical simulations.

### B. Film Coolant Pathlines

The film-coolant pathlines colored by the dimensionless temperature $\theta$ are shown in Fig. 8 for various film-hole arrangements with a blowing ratio $M = 1$. For the plane tips, the camber arrangement shows the coolant rolls around inside the plenum before exiting from the film holes located on the middle camber line of the blade tip. The coolant then mixes with the tip leakage flow by exchanging momentum and energy, travels across the suction-side portion of the blade tip, and rolls away from the suction side of the tip to form a leakage vortex in the cascade passage. On the other hand, the coolant jets in the upstream film-hole arrangement travel across the entire blade tip width before they roll down the suction side. It is quite clear that the upstream film-hole arrangement is able to provide complete coverage of the entire blade tip from the pressure side to the suction side. The two-row arrangement is a combination of the camber and upstream arrangements which splits the same amount of coolant into two parts. Some coolant was delivered from the film holes near the pressure side to cover the whole width of

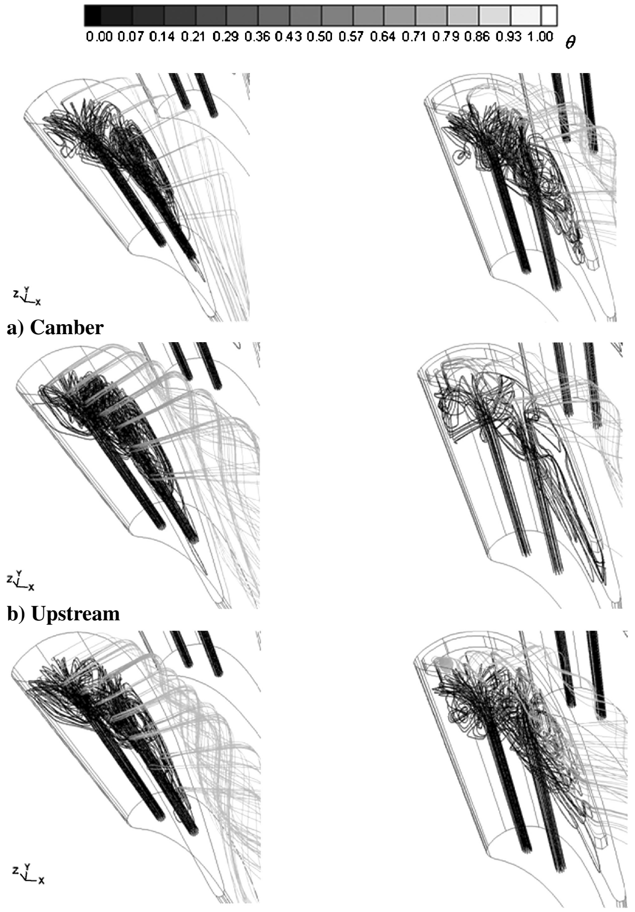


**Fig. 8 Film-coolant pathlines (shaded by dimensionless temperature $\theta$) among various low parameter film hole arrangements, $M = 1$ for camber and upstream configurations and $M = 0.5$ for two-row configuration: plane tip (left) and squealer tip (right).**

the blade tip, whereas the others were delivered from the middle camber line to cover only the suction-side portion of the blade tip.

For the squealer tip cases, the coolant flow structures are more complex in comparison with the plane tip cases. For the camber arrangement, the coolant rolls around inside the plenum similar to what was observed earlier for the plane tip case. The coolant then exits from the film holes at the bottom of the cavity and mixed with the tip leakage flows inside the squealer cavity. Some coolant near the trailing-edge portion rolls away from the suction rim directly; the remaining coolant travels downstream along the trailing direction and leaves the squealer tip to form a leakage vortex in the cascade passage. The upstream film-hole arrangement shows that more coolant is trapped in the leading-edge portion of the squealer cavity and that the coolant jets in the trailing edge region tend to cover a wider area of the blade tip and provide a better overall film-cooling effectiveness in comparison with the camber arrangement. For the two-rows film-hole arrangement, the pathlines are basically a combination of those generated by the camber and upstream arrangements with more balanced coverage between the leading-edge and trailing-edge portions of the blade tip.

Also note that the coolant jet pathlines for all three different film-hole arrangements roll away from the blade tip without touching the blade suction side when forming the leakage vortex in the cascade passage. This implies that film coolant jets protect only the blade tip and shroud regions, whereas the suction side of the blade surface below the blade tip does not benefit from the film cooling in these studies.

### C. Film-Cooling Effectiveness

Figure 9 shows a comparison of the calculated film-cooling effectiveness on the plane and squealer tips for different tip configurations with the measured PSP data of Ahn et al.[23] In general, the numerical results tend to overpredict slightly the film-cooling effectiveness downstream the film holes, but the effectiveness patterns match fairly well with the PSP data for both the plane and squealer tip cases. For the camber arrangement, the area protected by the film cooling begins from the camber line toward the suction-side edge on the plane tip. On the squealer tip, however, the film-coolant jets move from the camber line toward the pressure side and trailing edges with high film-cooling effectiveness on the pressure side downstream of the film holes. In general, the numerical results are closer to the PSP data of Ahn et al.[23] than the transient liquid crystal experimental data of Kwak and Han[18,19] shown in Fig. 1. Note that there are 13 film holes in the experimental study of Kawk and Han,[18,19] whereas the present film-hole configuration is identical to that used by Ahn et al.[23] with only 7 film holes.

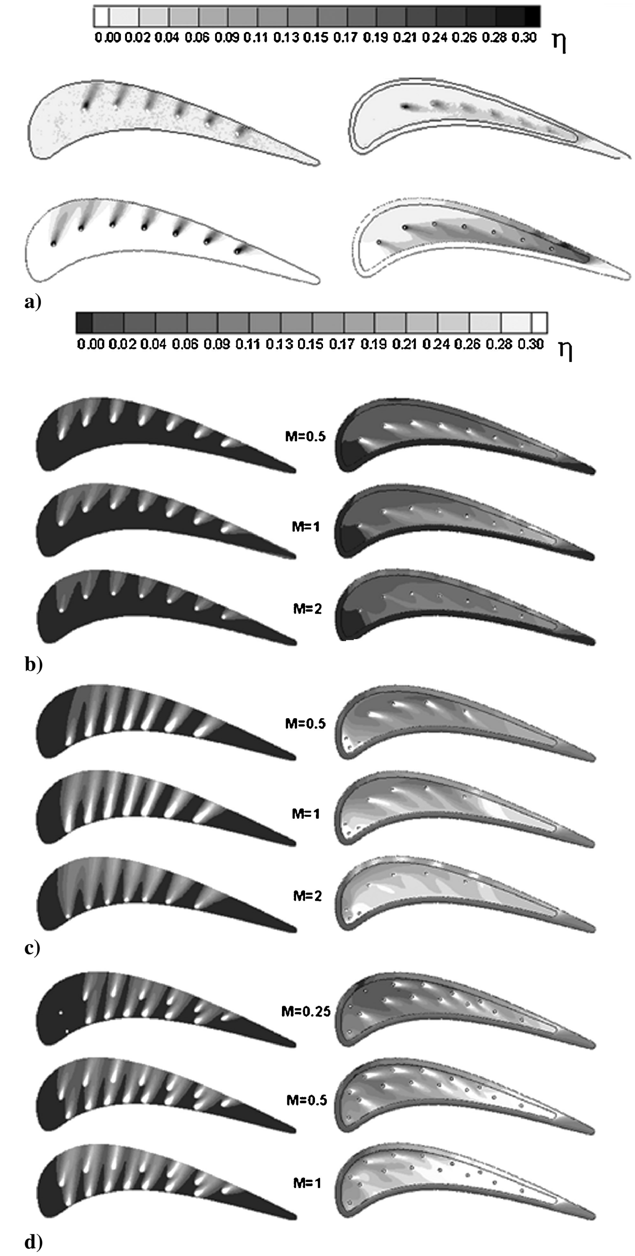


**Fig. 9 Film-cooling effectiveness on plane (left) and squealer (right) tips with various film-hole arrangements and blowing ratios, low parameter: a) $M$ = 1, top, experimental data by PSP, Ahn et al.,[23] and bottom, numerical simulation; b) camber; c) upstream; and d) two row.**

For completeness, the predicted film-cooling effectiveness on the plane and squealer tips with different film-hole arrangements and three blowing ratios of $M = 0.5$, 1, and 2 whereas $M = 0.25$, 0.5, and 1, respectively, for two-row configurations, are also shown in

Fig. 9. For plane tips, the patterns of film cooling effectiveness match the trajectories of the tip leakage flow, developing from the pressure-side edge and ending at the suction-side edge. Note that the upstream film-hole arrangement covers a wider area of the blade tip than the camber arrangement. For the squealer tips, the film-cooling effectiveness pattern at the bottom of the cavity develops from the camber line to the pressure side, which also matches the tip leakage flow inside the squealer cavity. As noted in earlier discussions, the camber arrangement only covers one-half of the blade tip portion. On the other hand, the upstream film-hole arrangement produced a better film-cooling effectiveness because the film holes are located on the upstream side of the leakage flow to protect more blade tip area. The two-row film-hole arrangement also provides better overall protection than the camber arrangement because some of the film holes were placed upstream of the leakage flow for more balanced coverage of the high heat transfer regions on the squealer tip.

For the range of blowing ratios considered here, the film-cooling effectiveness generally increases with increasing blowing ratio. However, as the blowing ratio increases for the camber arrangement on the plane and squealer tips, the coolant may separate from the blade tip surface and penetrate through the tip leakage flow rather than adhere to the blade tip. This results in a reduction of film-cooling effectiveness downstream of the film holes as shown in the bottom row of Fig. 9b for the $M = 2$ cases. Also to note from the top right of Fig. 9d that there is no film-cooling protection on the leading-edge portion of the plane tip for the two-row arrangement under a low blowing ratio $M = 0.25$. This suggests that the hot gas may enter the first two film holes under low blowing ratio conditions. To prevent this failure, it is desirable to use a higher blowing ratio for the two-row arrangement on the plane tip.

Figure 10 shows a comparison of the predicted film-cooling effectiveness on the shroud for the plane and squealer tip cases with camber, upstream, and two-row film hole arrangements under three different blowing ratios of $M = 0.5$, 1, and 2 (whereas $M = 0.25$, 0.5, and 1, respectively, for two-row configurations). For both the plane and squealer tip configurations, the film-cooling effectiveness on the shroud increases with increasing blowing ratio. This is different from the film cooling on the blade tip because the coolant penetrates the tip leakage flow and impinges directly on the shroud when the blowing ratio is high. For the plane tip configuration, the coolant traces on the shroud match closely with those observed on the blade tip, but the level of film-cooling effectiveness is directly opposite to that observed on the blade tip. More specifically, the low film-cooling effectiveness on the shroud corresponds to high cooling effectiveness on the blade tip and vice versa. For low blowing ratio cases, the film-cooling effectiveness on the shroud is lower than that observed on the blade tip because the coolant jets remain attached on the blade tip surface. With increasing blowing ratio, there is a drastic increase of the film-cooling effectiveness on the shroud because the coolant can easily penetrates the narrow tip gap. On the other hand, the film-cooling effectiveness on the shroud of the squealer tip is much lower than that on the blade tip because the cavity depth is relatively large. The coolant traces can no longer be seen because the coolant mixed well with the leakage flow inside squealer cavity before reaching the shroud. Also note that some regions of the shroud around the blade trailing edge and suction side also benefit from the coolant leakage vortices.

A detailed comparison of the area-averaged film cooling effectiveness on the blade tip is made in Fig. 11 to evaluate the overall performance of various film-hole arrangements. In general, the upstream and two-row film hole arrangements provide higher cooling effectiveness on blade tips than the camber arrangement for both the plane and squealer tips, especially for the high blowing ratio conditions. For the same amount of coolant usage, the squealer tip provides a better cooling effectiveness than the plane tip for two reasons: 1) lower tip leakage velocity for the squealer tip and 2) a large portion of the coolant is trapped in the squealer cavity as seen from the pathlines shown in Fig. 8.

Figure 11 shows a comparison of the area-averaged film-cooling effectiveness on the tips for various working conditions. As mentioned before, the blowing ratios for the two-row configurations are only one-half of the one-row configurations for the same amount of coolant. Generally speaking, the film-cooling effectiveness increases with increasing blowing ratio: The three exceptions are the camber arrangements for both the plane and squealer tip cases and

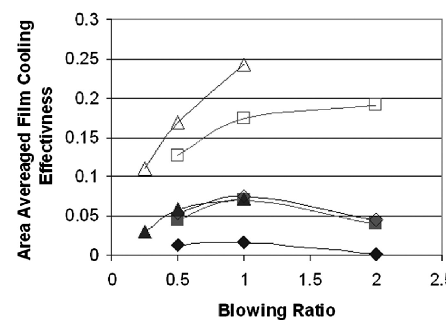


**Fig. 11 Area-averaged film-cooling effectiveness on blade tip with various tip configurations and film hole arrangements, low parameter, nonrotating: ◆, plane camber; ■, plane upstream; ▲, plane two row; □, squealer upstream; ◇, squealer camber; and △, squealer two row.**

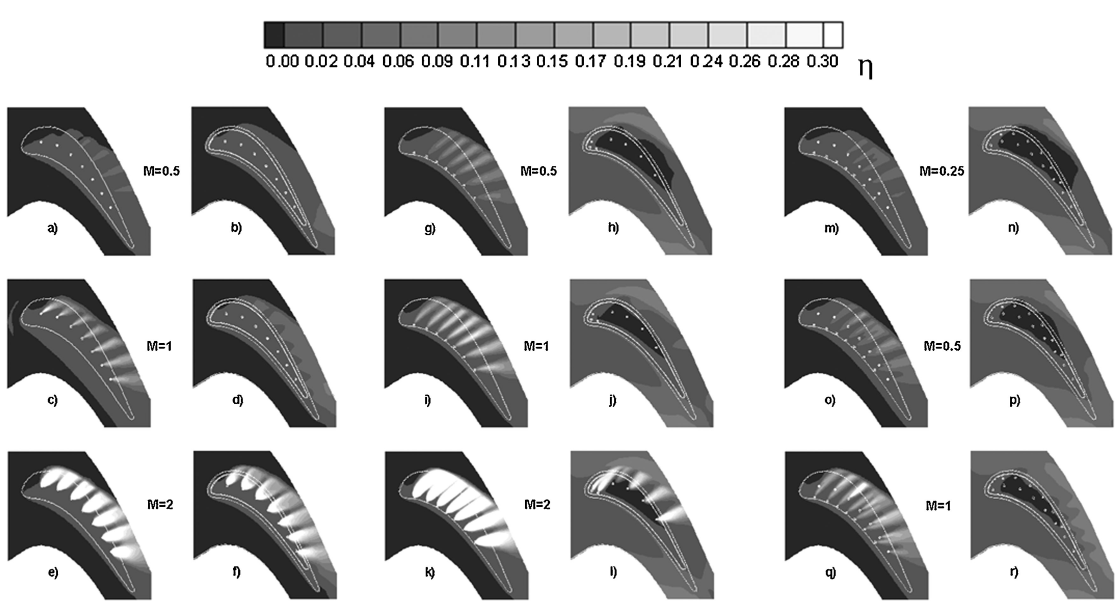


**Fig. 10 Film-cooling effectiveness on the shroud for plane and squealer tip configurations with various film-hole arrangements and blowing ratios, low parameter: a–f) camber, g–l) upstream, and m–r) two row.**

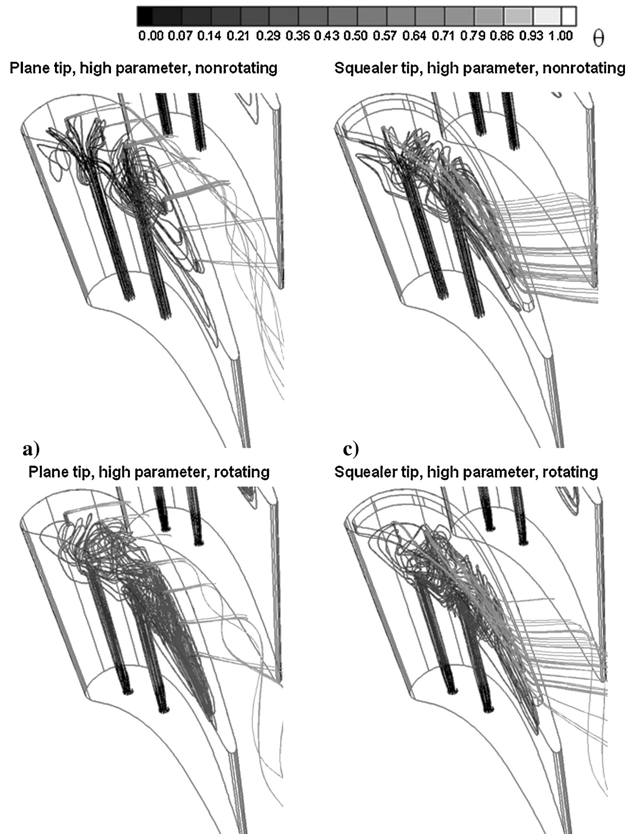


**Fig. 12 Coolant pathlines (shaded by dimensionless temperature), nonrotating and rotating cases, high parameter, $M = 1$.**

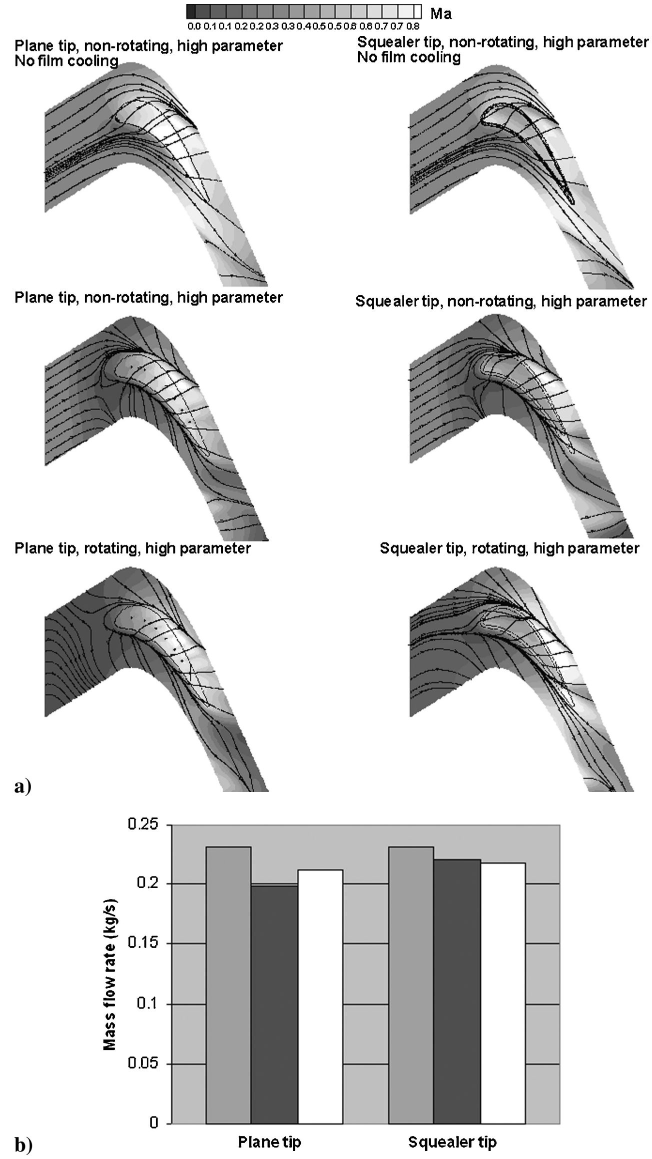


**Fig. 13 Comparison of a) streamlines, Mach number contours on midgap plane and b) tip leakage mass flow rate for ■ nonrotating no-film-cooling (Yang et al.[22]); ■, nonrotating film-cooling; and □, rotating film-cooling cases, high parameter conditions, $M = 1$.**

the plane tip upstream arrangement at the highest blowing ratio, of $M = 2$. For the camber arrangement of plane and squealer tip cases, the cooling effectiveness on the tips decreases after reaching a maximum value at around $M = 1$. At $M = 2$, the coolant jet lifts off from the blade tip and penetrates into the tip leakage flow with streamwise flow separation behind the coolant jets. Note that the two-row arrangement provides the highest film-cooling effectiveness at the highest blowing ratio, that is, $M = 1$, for both the plane and squealer tip configurations. This is because the two-row coolant holes split the coolant and reduce the local blowing ratio, so that the coolant tends to remain attached rather than penetrating the leakage flow for the range of blowing ratio considered. Also note that the squealer tip upstream arrangement also provides the highest cooling effectiveness at the highest blowing ratio, that is, $M = 2$, because the squealer tip is able to trap more coolant when the film holes are located in the upstream section of the squealer cavity.

### D. Effect of Rotation on Film-Cooling Effectiveness

Figure 12 shows a comparison of the coolant pathlines of camber configurations under nonrotating and rotating conditions for both the plane and squealer tip configurations at a blowing ratio of $M = 1$. In general, the rotation tends to reduce the size of the coolant leakage vortex in the suction-side passage because the blade is moving in the same direction as the tip leakage flow. As noted in a previous study (Yang et al.[22]) for blade tip heat transfer without film cooling, the rotating effect is confined to the shroud region and has relatively minor influence on the blade tips. Under the rotating conditions, the location of highest leakage flow shifts slightly downstream toward the trailing edge. However, the tip leakage flow is still dominated by the pressure gradient between the blade pressure and suction sides, and the coolant traces are only slightly affected by the blade rotation.

Figure 13 shows the effect of blade rotation on the streamlines and Mach number contours at the midgap plane and tip leakage flow rate for both the plane and squealer tip configurations. For completeness, calculations were also performed for the non-film-cooled plane and squealer tip configurations under the same flow conditions to facilitate a detailed comparison of the film cooling effects. It is seen that the tip leakage flow is driven from the pressure side to the suction side for both the plane and squealer tip configurations. The Mach number contours indicate that the squealer tip reduces the tip leakage flow compared to the plane tip in the midgap plane. For the film-cooling cases, the flow velocity reduces significantly at the midgap plane due to the blockage of the coolant jets. Furthermore, a portion of the midgap flow was deflected back to the pressure side, as indicated by the streamline convergence pattern in the pressure side of the turbine blade. For the plane tip configuration, the effects of film cooling can be clearly observed from the low-speed coolant traces at the midgap plane. On the other hand, the coolant traces are no longer visible for the squealer tip cases because the squealer cavity depth is considerably larger than the tip gap. This explains the difference of cooling effectiveness between plane and squealer tips shroud as shown earlier in Fig. 10. The bottom row of Fig. 13a shows the streamlines for the rotating cases in a blade-fixed frame. The streamlines outside the blade tip region are turning toward the pressure side relative to the rotating blade. However, the streamlines in the tip gap region are still moving from the pressure side to suction side because the leakage flow for rotating cases is still dominated by the pressure gradients. Note further that the blade rotation tends to increase the tip leakage flow near the blade trailing edge for both the plane and squealer tip configurations. A more detailed discussion of the rotating effects on the tip leakage flow is given by Yang et al.[22]

Figure 13b shows a comparison of the tip leakage flow rate for the plane and squealer tip configurations under various flow conditions. It is seen that the leakage mass flow rates are nearly identical for the non-film-cooled plane and squealer tips. Although the squealer tip reduces the leakage flow velocity in the squealer cavity, the overall leakage mass flow rate stays about the same due to increased cross-sectional area for the squealer tip configuration. Also note that the film cooling tends to reduce the leakage mass flow rates for both the plane and squealer tip configurations because the slower coolant jet act as a blockage to the tip leakage flow. For the film-cooled plane tip configuration, the blade rotation produced a significant increase of the leakage mass flow rate. On the other hand, the leakage flow rate for the squealer tip configuration is only slightly affected by the blade rotation at $M = 1$ because the coolant is not strong enough to penetrate the tip leakage flow at this blowing ratio.

Figure 14 shows the streamlines and dimensionless temperature contours at two streamwise cross sections for the plane and squealer tips under various flow conditions. Each cross section consists of two separate planes, that is, the pressure-side plane and suction-side

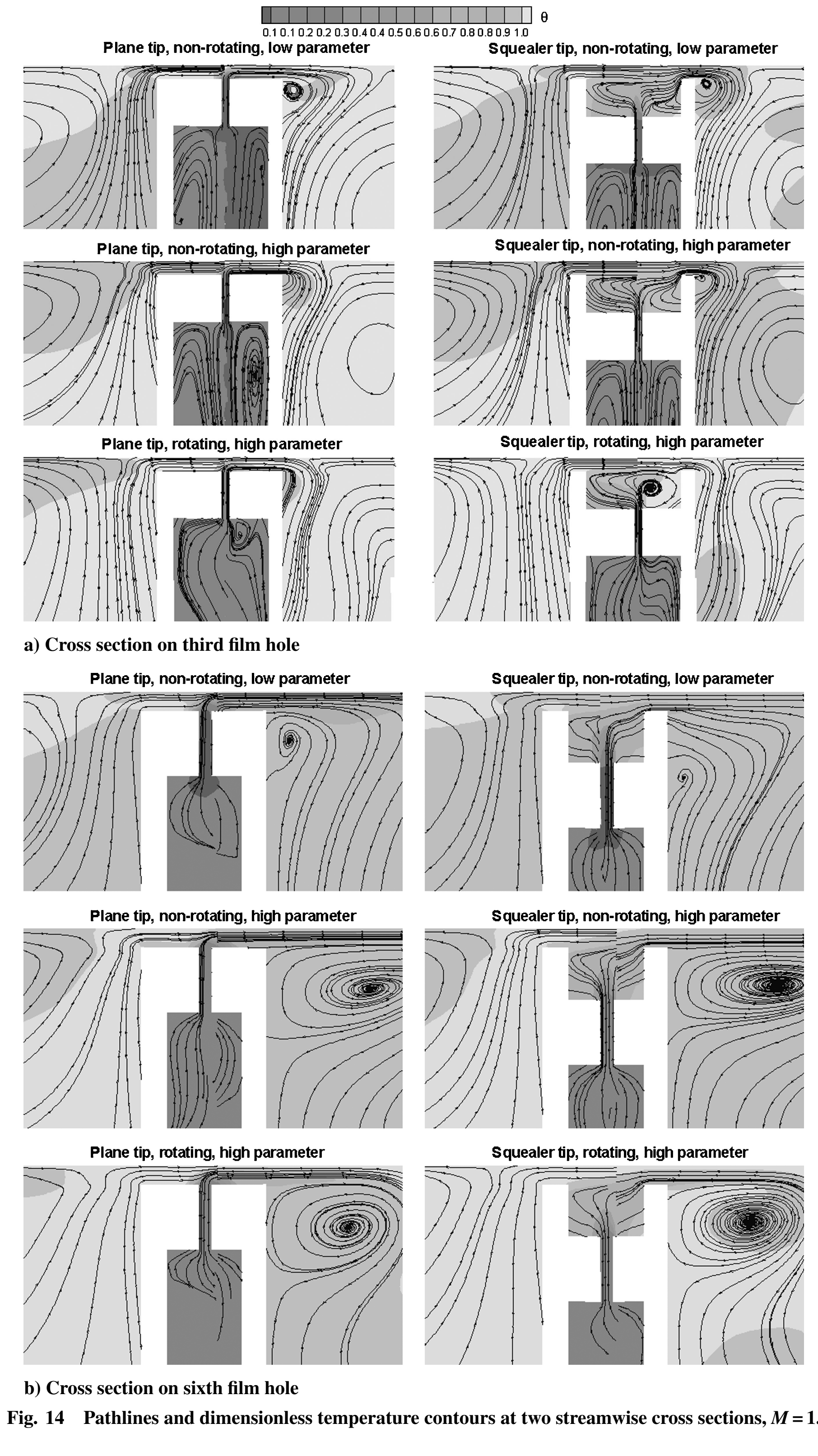


**Fig. 14 Pathlines and dimensionless temperature contours at two streamwise cross sections, $M = 1$.**

plane as shown in Fig. 4, which are perpendicular to the pressure side and suction side of the blade surface, respectively, and intersect at the camber line. It can be seen from Fig. 4 that the first cross section cuts through the center of the third film hole, the plenum, and the second coolant passage, whereas the second cross section cuts through the center of the sixth film hole and the tail end of the plenum. In general, all tip leakage flows were driven from the pressure side to the suction side by the blade pressure gradient between the pressure side and suction side of the blade. The squealer tip is found to reduce the leakage vortex due to flow separation and recirculation inside the squealer cavity.

As noted by Yang et al.[22] for the non-film-cooled blade simulations, the location of the strongest tip leakage flow shifts downstream under high parameter conditions. This results in a somewhat weaker vortex at the location of the third film hole and a much stronger and larger leakage vortex at the sixth film hole. Also note that the plenum flow patterns are drastically different between the third and sixth film holes. At the location of the third film hole, a large recirculation region is observed inside the plenum because the coolant exiting from the second coolant passage impinges directly on the top surface of the plenum. On the other hand, the plenum flow leaves the sixth film hole smoothly because the flow from the coolant passages must travel horizontally toward the tail end of the plenum before exiting the sixth film hole.

When the nonrotating and rotating tip leakage flow rate in Fig. 13 and the flow pattern in Fig. 14 are compared, it is quite clear that the blade rotation does not affect the tip leakage flow significantly because the leakage flow is still dominated by the blade pressure gradient under rotating conditions. At the location of the third film hole, as shown in Fig. 14a, the size of the leakage vortex reduces slightly for both the plane and squealer tip configurations. However, the secondary flow inside the squealer cavity is significantly altered with the formation of an additional vortex around the coolant jet exiting from the third film hole. At the second cross section around the sixth film hole in Fig. 14b, a somewhat stronger leakage vortex is observed for both the plane and squealer tip configurations due to an increase of tip leakage velocity near the trailing edge, as shown earlier in Fig. 13. Also note that the squealer cavity width is considerably narrower at the sixth film hole in comparison with that at the third film hole. Consequently, the effect of coolant jet on the squealer cavity temperature distribution is more pronounced near the blade trailing edge, as seen in the cooling effectiveness contours shown in Fig. 15.

Figure 15 shows a detailed comparison of the film-cooling effectiveness on the blade tips under various flow conditions. It is seen that the high parameter condition produces a slight increase of the film-cooling effectiveness on the blade tips for both the plane and squealer configurations due to the flow compressibility and viscous heating. As shown earlier in Fig. 13, the blade rotation shifts the location of the strongest tip leakage flow downstream toward the trailing edge. This leads to an increase of film-cooling effectiveness near the trailing edge and a significant reduction of the cooling effectiveness in the leading-edge and midchord sections for the plane tip configuration. On the other hand, the rotating effect for the squealer tip configuration is confined to the trailing edge. The film-cooling effectiveness on the floor of the squealer cavity is only slightly affected by the blade rotation because the tip leakage flow is relatively weak for the large cavity depth considered in the present study.

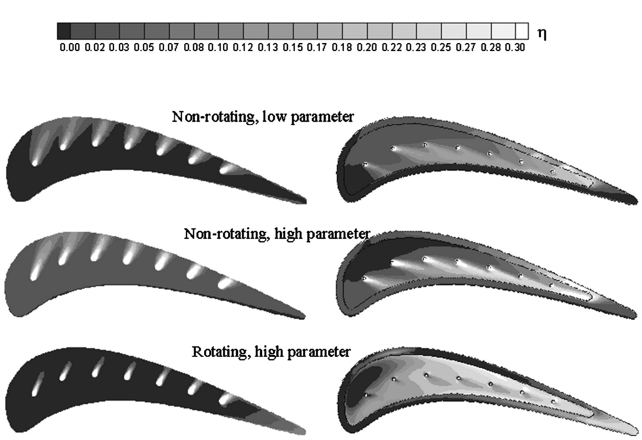


**Fig. 15 Film-cooling effectiveness comparison on plane (left) and squealer (right) tips for $M = 1$, various flow conditions.**

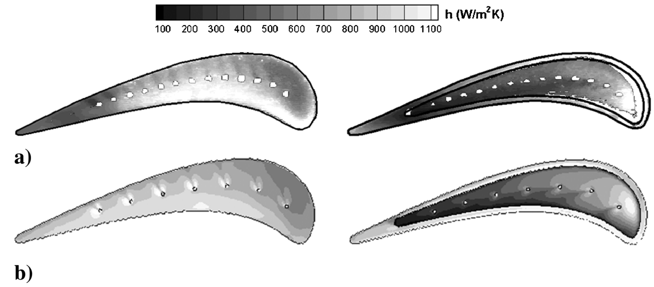


**Fig. 16 Heat transfer coefficients on the plane tip (left) and squealer tip (right) of camber arrangement, low parameter, $M = 1$: a) experimental data by LCT, $M = 1$, Kwak and Han[18,19] and b) numerical simulations.**

### E. Heat Transfer Coefficient of Film Cooling

Figure 16 shows a comparison of the predicted heat transfer coefficients for the camber line arrangement to the corresponding transient liquid crystal experimental data of Kwak et al.[18,19] for a blowing ratio of $M = 1$. As noted earlier, there are 13 film holes in the experimental configuration of Kwak et al.[18,19] but only 7 film holes were considered in the present simulations, although the blowing ratio is maintained the same. It is seen that the numerical simulation results are in good agreement in the pattern with the measured data for both the plane and squealer tips, although the numbers of film holes are different. Both the measurement and simulation results exhibit a low heat transfer coefficient downstream of the film holes, which is different from most of the other film-cooling applications with an increase of heat transfer coefficient as a result of film cooling. As shown earlier in Fig. 13, the tip leakage velocity in the narrow tip gap is significantly higher than the mainstream flow in the cascade. Therefore, the coolant velocity is considerably slower than the tip leakage flow velocity even at a blowing ratio of $M = 1$. Furthermore, the coolant jets are issued into the tip gap normal to the tip leakage flow instead of at an inclined angle to the blade tip. Consequently, the low-speed coolant jets act as a blockage instead of a turbulator to the tip leakage flow even at $M = 1$. This leads to a reduction of heat transfer coefficient downstream of the film holes for the plane tip configurations shown in the left column of Fig. 16. For the squealer tip configurations, the coolant blockage is not as strong as that for the plane tips because squealer cavity acts as a labyrinth seal to reduce the tip leakage flow. Therefore, the heat transfer coefficients on the squealer tip configurations do not clearly show a low heat transfer region downstream of the film holes.

Figure 17 shows a comparison of the Stanton number contours on the plane tip, squealer tip, and shroud for the nonrotating and rotating high parameter cases. In general, the blade rotation only slightly affects the heat transfer on both the plane and squealer tips. As noted earlier, the location of strongest tip leakage flow shifts toward the trailing edge under rotating conditions. A similar shift of the high heat transfer region is also observed in the Stanton number contours shown in Fig. 17. There is a minor reduction of Stanton number near the leading edge, whereas the Stanton number value increases slightly in the midchord and trailing-edge sections for both the pane and squealer tip configurations.

Unlike the blade tips, which are fairly insensitive to the blade rotation, the instantaneous Stanton number on the shroud is strongly affected by the blade rotation. For the plane tip configuration, the Stanton number increases due to a sharp increase of the velocity and temperature gradients inside the shroud boundary as a result of the blade rotation. On the shroud wall directly opposite to the plane tip, however, the Stanton number patterns are very similar to those observed on the blade tip because the tip leakage flow is nearly two dimensional in the narrow tip gap.

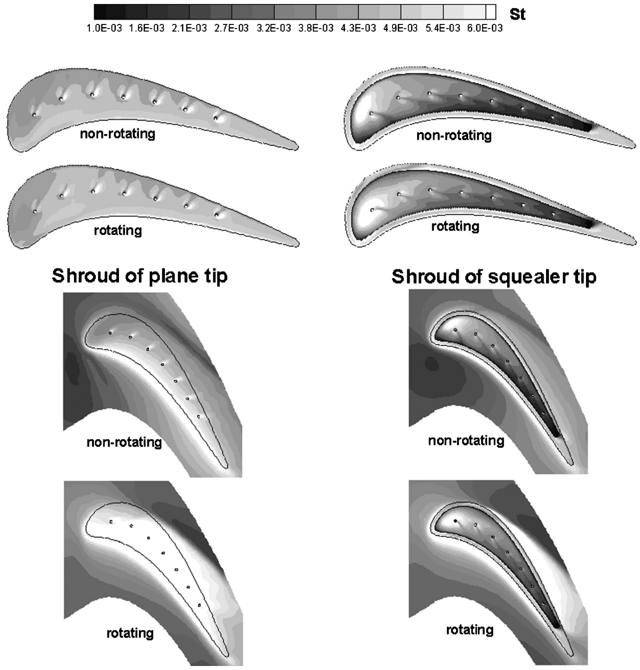


**Fig. 17 Instantaneous Stanton number contours on the plane (left) and squealer (right) tips and shrouds for high parameter, nonrotating and rotating cases.**

## V. Conclusions

Three different film-hole arrangements including camber (holes located at midcamber line), upstream (holes located upstream of the tip leakage flow and high heat transfer region), and two-row (combining upstream and camber arrangements) arrangements on the plane and squealer tips have been systematically investigated for both the low and high parameter, nonrotating and rotating conditions in this paper. Several major conclusions follow.

1) The blade tip film cooling does not affect the overall blade pressure ratio distribution significantly, except for the region downstream of the film holes.

2) The upstream and two-row arrangements provide better film-cooling performance on both the plane and squealer blade tips than the camber arrangement, especially at the high blowing ratios.

3) When the blowing ratio $M$ reaches 1, the film-cooling effectiveness ceases to increase for the camber arrangement on both the plane and squealer tips due to the coolant separation from the blade tip. However, the film-cooling effectiveness in the upstream and the two-row arrangements still tend to increase with higher blowing ratios.

4) The film-cooling effectiveness on the shroud depends mostly on the blowing ratio and is only slightly affected by the film-hole arrangements. The higher blowing ratio produces higher cooling effectiveness on the shroud for all cases considered.

5) For the range of blowing ratio considered in the present study, the coolant jets act as a blockage to the tip leakage flow. Therefore, low heat transfer coefficient is dictated downstream of the film holes on plane, squealer tips, and squealer shroud.

6) The rotation reduces the film-cooling effectiveness on the plane tip significantly, whereas the film-cooling effectiveness on the squealer tip is only slightly affected due to the large cavity depth.

7) The rotation significantly increases the heat transfer coefficient on the shrouds due to the increasing velocity and temperature gradient inside the shroud boundary layer.

8) The simulation shows that the blade suction side does not benefit from the tip film cooling for all cases considered.

9) The film cooling reduces the tip leakage mass flow rate for both the plane and squealer tip configurations. The squealer tip reduces the leakage flow velocity, but the overall leakage mass flow rate increases for the film-cooled cases due to increased flow area in the squealer cavity.

## Acknowledgment

The project was partially supported by the U.S. National Science Foundation under Grant CTS-9903972.

## References

[1]Metzger, D. E., Bunker, R. S., and Chyu, M. K., "Cavity Heat Transfer on a Transverse Grooved Wall in a Narrow Flow Channel," *Journal of Heat Transfer*, Vol. 111, No. 1, 1989, pp. 73–79.

[2]Chyu, M. K., Moon, H. K., and Metzger, D. E., "Heat Transfer in the Tip Region of Grooved Turbine Blades," *Journal of Turbomachinery*, Vol. 111, No. 2, 1989, pp. 131–138.

[3]Kim, Y. W., Abdel-Messeh, W., Downs, J. P., Soechting, F. O., Steuber, G. D., and Tanrikut, S., "A Summary of the Cooled Turbine Blade Tip Heat Transfer and Film Effectiveness Investigation Performed by Dr. D. E. Metzger," American Society of Mechanical Engineers, Paper 94-GT-167, June 1994.

[4]Bunker, R. S., Baily, J. C., and Ameri, A. A., "Heat Transfer and Flow on the First Stage Blade Tip of a Power Generation Gas Turbine: Part 1: Experimental Results," *Journal of Turbomachinery*, Vol. 122, No. 2, 2000, pp. 272–277.

[5]Bunker, R. S., and Baily, J. C., "Effect of Squealer Cavity Depth and Oxidation on Turbine Blade Heat Transfer," American Society of Mechanical Engineers, Paper 2001-GT-0155, June 2001.

[6]Dunn, M. G., and Haldeman, C. W., "Time-Averaged Heat Flux for a Recessed Tip, Lip, and Platform of a Transonic Turbine Blade," *Journal of Turbomachinery*, Vol. 122, No. 4, 2000, pp. 692–697.

[7]Bunker, R. S., "A Review of Turbine Blade Tip Heat Transfer," *Annals of the New York Academy of Sciences*, Vol. 934, 2001, pp. 64–79.

[8]Azad, G. M. S., Han, J. C., and Teng, S., "Heat Transfer and Pressure Distribution on a Gas Turbine Blade Tip," American Society of Mechanical Engineers, Paper 2000-GT-194, June 2000.

[9]Azad, G. M. S., Han, J. C., and Boyle, R., "Heat Transfer and Pressure Distribution on the Squealer Tip of a Gas Turbine Blade Tip," American Society of Mechanical Engineers, Paper 2000-GT-195, June 2000.

[10]Saxena, V., Nasir, H., and Ekkad, S. V., "Effect of Blade Tip Geometry on Tip Flow and Heat Transfer for a Blade in a Low Speed Cascade," American Society of Mechanical Engineers, Paper GT-2003-38176, June 2003.

[11]Kwak, J. S., Ahn, J., Han, J. C., Lee, C. P., Bunker, R. S., Boyle, R., and Gaugler, R., "Heat Transfer Coefficients on the Squealer Tip and Near Tip Regions of a Gas Turbine Blade with Single or Double Squealer," American Society of Mechanical Engineers, Paper GT-2003-38907, June 2003.

[12]Ameri, A. A., Steinthorsson, E., and Rigby, D. L., "Effect of Tip Clearance and Casing Recess on Heat Transfer and Stage Efficiency in Axial Turbines," *Journal of Turbomachinery*, Vol. 121, No. 4, 1999, pp. 683–693.

[13]Ameri, A. A., and Rigby, D. L., "A Numerical Analysis of Heat Transfer and Effectiveness of Film Cooled Turbine Blade Tip Model," NASA CR, 99-209165, June 1999.

[14]Ameri, A. A., and Bunker, R. S., "Heat Transfer and Flow on the First Stage Blade Tip of a Power Generation Gas Turbine: Part 2: Simulation Results," *Journal of Turbomachinery*, Vol. 122, No. 2, 2000, pp. 272–277.

[15]Ameri, A. A., "Heat Transfer and Flow on the Blade Tip of a Gas Turbine Equipped with a Mean-Camberline Strip," *Journal of Turbomachinery*, Vol. 123, No. 4, 2001, pp. 704–708.

[16]Yang, H., Acharya, S., and Ekkad, S., "Flow and Heat Transfer Predictions of a Plane Tip Turbine Blade," American Society of Mechanical Engineers, Paper 2002-GT-30190, June 2002.

[17]Yang, H., Acharya, S., and Ekkad, S., "Numerical Simulation of Flow and Heat Transfer past a Turbine Blade with a Squealer Tip," American Society of Mechanical Engineers, Paper 2002-GT-30193, June 2002.

[18]Kwak, J. S., and Han, J. C., "Heat Transfer Coefficient and Film Cooling Effectiveness on a Gas Turbine Blade Tip," American Society of Mechanical Engineers, Paper GT-2002-30194, June 2002.

[19]Kwak, J. S., and Han, J. C., "Heat Transfer Coefficient and Film Cooling Effectiveness on the Squealer Tip of a Gas Turbine Blade," American Society of Mechanical Engineers, Paper GT-2002-30555, June 2002.

[20]Acharya, S., Yang, H., and Ekkad, S., "Numerical Simulation of Film Cooling on the Tip of a Gas Turbine Blade," American Society of Mechanical Engineers, Paper GT-2002-30553, June 2002.

[21]Hohlfeld, E. M., Christophel, J. R., Couch, E. L., and Thole, K. A., "Predictions of Cooling Flow Dirt Purge Holes Along the Tip of a Turbine Blade," American Society of Mechanical Engineers, Paper GT-2003-38251, June 2003.

[22]Yang, H., Chen, H.-C., and Han, J.-C., "Flow and Heat Transfer on Turbine Rotor with Various Tip Configurations," *Journal of Thermophysics and Heat Transfer*, Vol. 20, No. 1, 2006, pp. 80–91.

[23]Ahn, J., Mhetras, S. P., and Han, J. C., "Film Cooling Effectiveness on a Gas Turbine Blade Tip and Shroud Using PSP," American Society of Mechanical Engineers, Paper GT-2004-53249, June 2004.

[24]Fluent User's Guide [CD-ROM], Ver. 6.1, Fluent, Inc., Lebanon, NH, 2003.